Applied Surface Science 641 (2023) 158462

Contents lists available at ScienceDirect

Applied Surface Science

journal homepage: www.elsevier.com/locate/apsusc

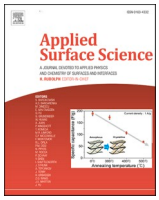

Full Length Article

Reframing ice adhesion mechanisms on a solid surface

Luca Stendardo [a,b], Giulia Gastaldo [b], Marc Budinger [c], Valérie Pommier-Budinger [b], Irene Tagliaro [a], Pablo F. Ibáñez-Ibáñez [a,d], Carlo Antonini [a,*]

[a] Department of Materials Science, University of Milano – Bicocca, via R. Cozzi 55, 20125 Milano, Italy
[b] ISAE-SUPAERO, Université de Toulouse, 10 Avenue Edouard Belin, 31400 Toulouse, France
[c] ICA, Université de Toulouse, UPS, INSA, ISAE-SUPAERO, MINES-ALBI, CNRS, 3 rue Caroline Aigle, 31400 Toulouse, France
[d] Department of Applied Physics, University of Granada, Campus de Fuentenueva, 18071 Granada, Spain

ARTICLE INFO

Keywords:
Ice adhesion
Icephobicity
Icing
Coatings

ABSTRACT

Mitigating icing hazards is of interest for many technological applications. One solution is to employ low ice adhesion coatings, either passively or in combination with active de-icing systems. Nevertheless, comparing different low ice adhesion surfaces can be challenging. Studies generally report the average shear stress, calculated as the ratio of applied force to the ice-substrate contact area; however, the fracture mechanism at the ice-substrate interface is rarely reported. There are two fracture mechanisms that can occur at the interface: stress-dominated and toughness-dominated. Average shear stress is only meaningful when performing adhesion tests in a stress-dominated regime; otherwise, interface stresses are underestimated and misleading. This study presents a new understanding of ice adhesion mechanisms combining experimental and numerical methods, demonstrating how the traditional ice adhesion reporting method can lead to errors up to 400%. Using a simple fracture model, the study shows that the stress-dominated fracture regime in the horizontal push test is favored by smaller ice diameter and greater ice thickness, and is also affected by the load force position. The identification of the two fracture regimes is required for the correct understanding and reproducibility of ice adhesion results, enabling better design and characterization of icephobic coatings and materials.

1. Introduction

The formation of ice on exposed surfaces represents a serious hazard to the safety and operation of instruments and facilities, such as aircraft [1-3], power lines [4], off-shore platforms, wind turbines, and solar panels [5]. The considerable societal and economic consequences of ice accretion have led to the development of various anti-icing and de-icing strategies [6], which traditionally include mechanical (pneumatic, expulsive, or vibratory), thermal (hot gas/bleed air or electrothermal melting) and chemical means (glycol-based anti-freeze liquids).

In the last fifteen years, research has been increasingly directed toward icephobic coatings [7–13]. Typically, these coatings are meant to be integrated with the above-mentioned strategies [14], introducing at least one of the following functionalities: high water repellence, i.e. superhydrophobicity [15–22], to promote liquid removal before freezing [23,24], freezing delay [25–27], freezing point depression, and low ice adhesion [28,29]. The interplay of icephobic surfaces with active anti-icing and de-icing strategies can significantly reduce the power consumption of ice protection systems (IPS) and reduce greenhouse gas emissions [30–32].

Over the years, different strategies for lowering ice adhesion strength on surfaces have been developed. The different typologies of anti-icing surfaces can be summarized in four categories: smooth, textured (i.e., hierarchical hydrophobic surfaces) [33,34], slippery [35–37], and subsurface textured surfaces [8,38–43].

1.1. Background

To compare the icephobic properties of the developed surfaces, similar test methods and conditions should be chosen. Many different test methods are found in the literature (e.g., centrifuge adhesion test, push or pull test, rotational shear test, lap shear test, and beam test) [44], and the data from different test benches are usually not directly comparable. Further problems arise when tests operate under different environmental conditions, when the ice formation procedure changes, or when ice samples of different types and sizes are used [45].

* Corresponding author.
E-mail address: carlo.antonini@unimib.it (C. Antonini).

https://doi.org/10.1016/j.apsusc.2023.158462
Received 26 July 2023; Received in revised form 7 September 2023; Accepted 9 September 2023
Available online 11 September 2023

The two most common test systems in literature are the centrifuge adhesion test and the horizontal push (or shear) test [44]. In particular, the horizontal shear test is relatively easy to build and allows for additional control over the ice detachment conditions compared to the centrifugal test (a direct mechanical connection to ice allows to record strain rates and ice creeping effects). As shown by [35,46–49], this type of test systems can be very simple and intuitive to set up; however, one considerable drawback is that it creates major stress concentrations at the ice-substrate interface. It was pointed out by [44,47,50], that the traditionally used average critical shear stress, defined as $\tau_{ave} = F/A$, where F is the removal force and A the area of the ice-substrate interface, should always be given specifying the test conditions. Depending on the test geometry, the maximum and minimum stress values can deviate significantly from the average shear stress calculated as $\tau_{ave} = F/A$, leading to an incorrect estimation of the critical stress value τ_c. When performing adhesion tests, the stress concentration factor [51] should be known or estimated by numerical analysis (e.g FEM) [44].

In the field of fracture mechanics, various techniques are available to characterize the strength of bonded joints [52]. Among ice adhesion studies, the stress approach is the most used, where the interfacial adhesive strength is expressed in terms of the maximum stress reached before failure of the joint. An interfacial fracture, however, can also be described in terms of energy, an approach that relies on linear elastic fracture mechanics. The maximum amount of strain energy that can be stored before failure of the joint is defined as "toughness" [52,53].

It has been previously shown [54] that, depending on the size of the ice-substrate interface, ice detachment can be dominated by stress or by toughness. In a stress-dominated detachment, the interface fails because the critical stress level is reached, while for a toughness-dominated fracture, the critical quantity is the strain energy [55] (refer to section 2.3). As a consequence, a measure of the critical shear stress is only meaningful if the ice detaches due to a stress-dominated fracture [52]. Additionally, section 2.3 of this work attempts to shed light on the often-ignored crack opening modes in the context of the push adhesion test. For the correct characterization of shear adhesion strength, understanding and recognizing the dominant crack opening mode is essential.

The authors believe that the above-mentioned considerations should be made to accurately assess the ice adhesion strength. The literature has shown that these parameters are important [44], however, they are often neglected in many well-cited papers of recent years as shown in Table 1.

1.2. Research approach

The goal of this work is to obtain a better and deeper understanding of the ice-substrate fracture mechanics for the horizontal push test: Specifically, we show how the average critical shear stress τ_{ave} depends on the testing conditions and should not be considered as an absolute surface property; nonetheless, τ_{ave} can be valuable information in comparative measurements, once the detachment mechanism has been identified. A hybrid experimental and numerical approach is used to investigate the stress distribution along the interface, showing how fundamental parameters such as pusher height or ice block diameter influence the measured critical shear stress.

In general, the fracture of a bi-material interface can be dominated by stress or toughness [53,57,58]. Here, a finite element analysis is used to calculate the change of strain energy during crack propagation and predict whether the fracture is stress- or toughness-dominated. Additionally, it is shown that, in a stress-dominated fracture mechanism, the relevant value that characterizes a surface is the minimum stress value over the entire interface. A mechanical framework for the horizontal push test is then derived, allowing the definition of the ideal test conditions and methods for critical shear stress measurements.

As a result of this analysis, the proposed research approach is summarized in Fig. 1, representing a flow chart of ice adhesion measurement steps. The general process is valid for all kinds of test setups: however, in this study, it has been applied to the horizontal push test. The input parameters of the workflow are the test system design rules presented in section 2.3, and the Shear Stress Intensity Factors, derived and presented in section 2.1.

This work attempts to create awareness of the common mistakes and misconceptions related to ice adhesion testing on the horizontal push test. More reliable and reproducible tests are relevant for the design and fabrication of coatings and materials based on low ice adhesion to contrast icing.

2. Materials and methods

2.1. Experimental section

The experimental test method used for this study is the horizontal shear (or push) test. An in-house designed test rig composed of four main elements (environmental chamber, cooling system, force sensor, and actuation system) is used (Fig. S1a of Supporting Information SI). A liquid-cooled, thermoelectric system is used to bring the substrates to subzero temperatures (Fig. S1b). The cooling system is placed inside the environmental chamber, which is equipped with a continuous nitrogen gas supply (ambient temperature $T_{amb} = 20^{\circ}C$, relative humidity $RH < 3\%$). During ice formation and testing, the substrate temperature is set to -10 °C and controlled by a PID-Controller with a 5 K-Ω thermistor (TE Technology, Inc.). To form the ice on the substrate, cylindrical nylon (PA.6) cuvettes (inner diameter 8 mm or 14 mm) are used. Water is poured into the cuvettes and then cooled down to the predefined freezing temperature. The ice adhesion tests are conducted after at least 20 min of conditioning time to ensure a complete freezing of the water column.

A force applied parallel to the substrate on the outside of the nylon cuvette induces stress at the ice-substrate interface. A linear displacement system (Newport LTA-HL with Conex-CC Controller) is used to move a force gauge (Mark-10 model M5-20) toward the ice column. The force gauge is equipped with a metallic rod that pushes the nylon cuvette, while the applied force is recorded by the gauge. The linear actuator moves with a constant velocity and, therefore, increases the applied force on the ice linearly. In this study, the actuation speed is set to 10 μm/s, a quasi-static regime where dynamic effects can be excluded (see Figure S2). This study is carried out using a commercially available

Table 1
Summary of parameters and tools that need to be considered for accurate critical shear stress measurement using a horizontal push test. A comparison between important studies of the recent year is proposed. The symbol "✓"indicates that the item is included in the study, while "×"indicates that the item was not considered or reported.

	Considers τ and σ	Pushing height	Stress distribution	Stress vs. toughness	FEM	Crack opening mode
Lou et al. [51]	×	×	✓	✓	✓	×
Maitra et al. [47]	✓	✓	×	×	×	×
Makkonen [50]	×	–	✓	✓	✓	×
Golovin et al. [53]	×	×		✓	×	×
Irajizad et al. [42]	×	✓	×	×	×	×
Huré et al. [56]	×	×	✓	✓	✓	✓
This study	✓	✓	✓	✓	✓	✓

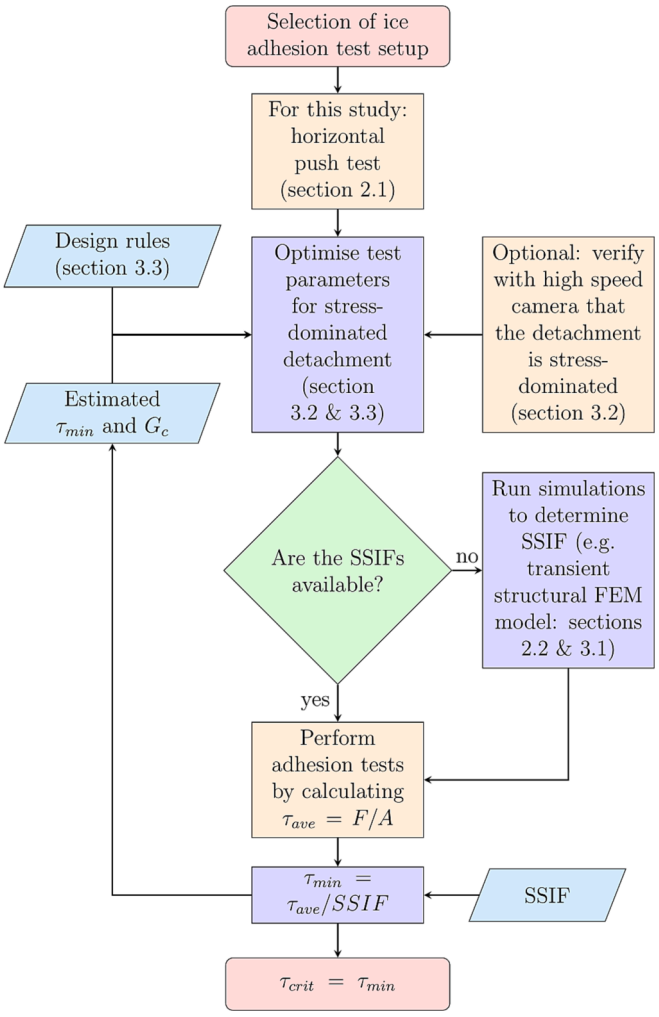

Fig. 1. Flow chart for the proposed research approach, aiming at increasing the accuracy of critical shear stress measurements (τ_{crit}) with the horizontal push test. The orange boxes represent experimental steps, the ones in blue are numerical steps, and the input and output parameters are represented in cyan. The design rules of section 2.3 and the concept of Shear Stress Intensity Factors (section 2.1) are used as input to the workflow.

standard material (Al-6060 aluminum alloy) as a sample surface.

2.2. Numerical model

A numerical FEM model is used to compute the interface stresses and strain values for the given experimental setup. The model is composed of three elements: the ice column, the nylon cuvette, and the aluminum substrate (see Section S3). Similar to the experimental setup, the force is applied on the outside of the cuvette, on an area with dimensions 1×1 mm^2, corresponding approximately to the contact area between the head of the rod and the nylon cuvette. The chosen elastic material properties are shown in Table 2.

To retrieve the ice-substrate stresses, a transient structural model is chosen (Ansys Mechanical 2020 R1). Validation of the model can be found in Section S4 of the SI. The forces measured with the experimental setup at the moment of detachment are used as an input parameter for the structural model, which returns the interface stress values for the given force. On the other hand, the strain energy release rate values are computed according to the method described in [60] and [52], by calculating the difference of strain energy for a variable crack length. The contribution of each of the different crack opening modes [61] is calculated by using the Virtual Crack Closure Technique (VCCT) [62].

Table 2
Density, elastic modulus, and Poisson's ratio of the modeled materials. The values of ice correspond to those of "freezer ice"[59].

Material	ρ (kg/m^3)	E (GPa)	ν
Aluminum	2700	68	0.36
Nylon	1140	1.5	0.39
Ice	897	9	0.31

2.3. Theoretical background

Detachment of ice can be explained by considering two competing fracture criteria: critical stress and critical strain energy (or toughness) [52–54,56]. Analytical models presented in [63] have shown that for relatively small interfaces, detachment is typically controlled by the critical shear stress of the interface. In these conditions, rupture occurs instantaneously along all the interface and, consequently, the stress level needs to exceed the critical value in each position x of the ice-substrate interface S (Fig. 2a) [52]:

$$\tau > \tau_c, \forall x \in S \tag{1}$$

On the other hand, for large interfaces, ice detachment is controlled by critical strain energy or "toughness" [53]. In this case, a crack is initiated by an opening of finite area $\Delta S < S$ (Fig. 2b), where the following relations hold [52]:

$$\tau > \tau_c, \forall x \in \Delta S \tag{2}$$

$$-\Delta E \geq G^c \Delta S \tag{3}$$

Here, $-\Delta E = E(0) - E(S)$ denotes the difference of the potential strain energy and $G^c \Delta S$ is the energy dissipated during crack onset (G^c is the critical strain energy or fracture toughness). For crack initiation to occur, relations (2) and (3) must hold at the same time. This condition is known as the "coupled criterion" and has been described in detail by Leguillon and co-workers in [52] and [55].

In the general case of crack initiation, an interface may be subjected to different types of loading, which involve different relative movements of the cracked surfaces. Three different crack opening modes can be identified [61]: (I) opening, (II) sliding or in-plane shear, and (III) tearing or out-of-plane shear (Fig. 2c). According to Huré et al. [56], when a crack appears at the interface of two different materials, the crack path is constrained and not free to propagate in a pure opening mode (I), as would be the case for a homogeneous material. In this case,

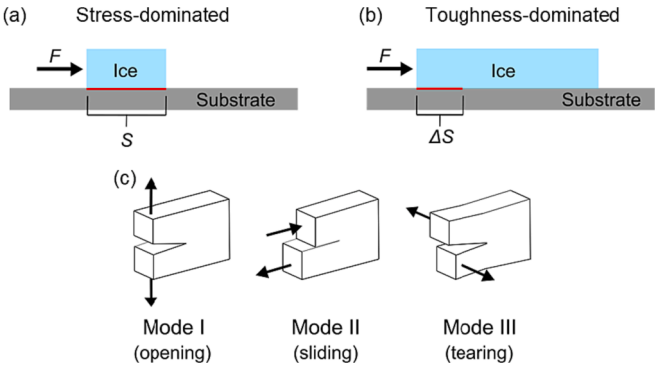

Fig. 2. (a) Stress-dominated detachment. For small interfaces, detachment is controlled by the critical shear stress of the interface. In these conditions, instantaneous rupture along the entire interface occurs. (b) For larger interfaces, detachment is controlled by critical strain energy or "toughness". Typically, in this case, a crack is initiated by an opening of finite area $\Delta S < S$. (c) Schematic representation of three different failure modes: (I) opening, (II) sliding or in-plane shearing, and (III) tearing or out-of-plane shearing.

crack propagation occurs in a mixed mode, generally opening (I) and sliding (II) mode [64]. When designing ice-adhesion experiments, it is therefore essential to understand and recognize which is the dominant mode occurring during the test. As discussed in the results, if the objective of the experiment is to measure the critical shear stress of the interface, then a configuration where the sliding (II) mode is dominant should be chosen.

3. Results and discussion

3.1. Determination of the failure criterion

The investigation of the stress states and understanding of the detachment mechanisms in the horizontal push test start from the analysis of the parameters involved in tests with cylindrical samples of bulk ice. A schematical representation of the test system is depicted in Fig. 3a. After the freezing process has been completed, a force probe is used to detach the ice from the substrate. To obtain the ice adhesion values, molds of inner diameters, *D,* of 8 and 14 mm are used, and the pushing force is applied at different heights *h*. It is expected that varying the distance *h* changes the entity of the stress components at the ice-substrate interface, as the bending moment is increased with increasing distance *h*.

The results of this study are summarized in Fig. 3b, where the average critical shear stress $\tau_{ave} = F/A$ is plotted as a function of the pushing height *h* and of the mold diameter *D*. In this case, the force *F* [N] at which the ice is detached from the substrate is divided by the ice-substrate contact area *A* [m^2]. It can be noticed that the average critical shear stress value of the interface decreases with increasing distance *h*. As the pushing location changes, the distribution of the stress components varies, thus resulting in different average critical shear stress values.

Calculating the average critical shear stress as F/A is common practice in the literature to account for different sizes of the ice-substrate interface. However, by comparing the average critical shear stress obtained with an 8 mm mold to that of a 14 mm mold, τ_{ave} ranges from 1257 ± 279 kPa to 358 ± 69 kPa, respectively, a 4x difference. Without any special attention to the execution of the test, the horizontal push test does not provide a unique value of the critical shear stress of the interface. By using the same substrate, the same environmental conditions, and by just slightly changing the configuration of the test system, up to 4 times higher ice adhesion values are observed. Taking this into account, comparing ice adhesion values from different test benches seems even more problematic.

To have a better understanding of the stress components at the ice-substrate interface when performing this kind of ice adhesion measurement, a numerical FEM model is developed. Fig. 3c shows the deformation of the mold ($D = 8$ mm) and the ice block ($H = 10$ mm) when the force is applied at the lowest application point considered in this study ($h = 1$ mm). The magnitude of the force applied in the numerical model is equal to the experimental average value for ice detachment at the same pushing height. The color contours reveal that even at this low pushing height, there is a clear bending of the mold and the ice block, as the displacement from the starting position increases when moving further away from the substrate.

The numerical model also allows plotting the in-plane shear and tensile stresses at the ice-substrate interface. The shear stresses for $h = 1$ mm and $h = 4$ mm have been plotted in Fig. 3d, for a load leading to detachment. Since both plots follow the same color scheme, it can be appreciated how there are much higher stress concentrations close to the force application point for $h = 1$ mm. The maximum shear stress values in the interfaces are therefore different from each other, showing that these values cannot be used as a failure criterion.

The ice sample size used in this study (cylindrical ice column with a

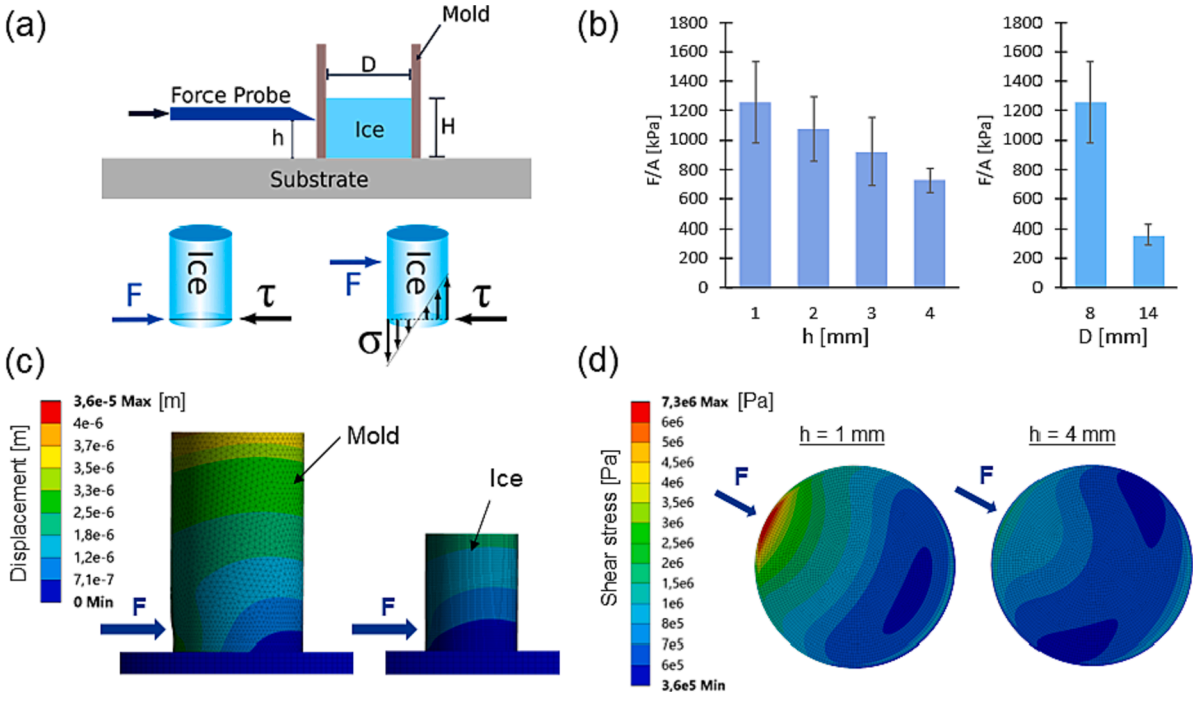

Fig. 3. (a) Schematic of the horizontal push test with bulk ice. The mold has an inner diameter *D* and the height of the ice is denoted by *H*. The force probe pushes at a finite height *h* from the substrate against the mold containing the ice. Depending on the distance *h*, the stress composition (shear stress τ and tensile stress σ) at the ice-substrate interface changes. (b) Experimental ice adhesion results for different pushing heights *h* (left graph, for constant $D = 8$ mm) and different mold diameters *D* (right graph, for constant $h = 1$ mm). The average critical shear stress has been calculated as the ratio of the applied force *F* at the moment of detachment by the contact area *A*. (c) Numerical representation of the displacement of the mold ($D = 8$ mm) and the ice bulk ($H = 10$ mm) when the load is applied. For illustration purposes, the displacements have been magnified 30 times. (d) Shear stress distribution at the ice-substrate interface for $h = 1$ mm and for $h = 4$ mm, with $D = 8$ mm in both cases. The stresses have been computed for a load leading to detachment (determined in (b).

diameter $D = 8$ mm) is relatively small compared to other similar test rigs found in the literature. According to the theories in [53,54,56,63], one would expect a stress-dominated debonding for this particular test case. A necessary condition for this debonding mechanism would be that in all 4 cases, one of the stress components (shear or tension) reaches the critical stress level over the whole ice-substrate interface. To understand this mechanism more in detail, an in-depth analysis of the individual stress components is proposed.

Fig. 4a and b plot the numerically calculated shear and tensile stresses along the centerline of the ice-substrate interface in the case of a mold with diameter $D = 8$ mm (Fig. 4, inset). The Z-coordinate describes the position along the centerline, with Z = −0,004 m being the closest to the force application point and Z = 0,004 m the farthest. Each line corresponds to the stress distribution for the force, experimentally determined, needed to detach the ice. Mesh independence is confirmed and is presented in the SI (Section S5).

The maxima of the shear stress curves in Fig. 4a at location Z = -0,004 m vary from 1,09 MPa for $h = 4$ mm to 5,46 MPa for $h = 1$ mm, which corresponds to a relative difference $\Delta\tau_{max}/\tau_{max} = 401\%$. The minimum values, on the other hand, go from 588 kPa for $h = 1$ mm to 675 kPa for $h = 3$ mm, with a relative difference of only $\Delta\tau_{min}/\tau_{min} = 14\%$. The complete results are summarized in Table 3. This way, the minimum shear stress seems to be the common stress state among all the considered cases. As described in [53,55], in a stress-dominated fracture mechanism the critical stress needs to be exceeded over the whole interface. Therefore, what should be considered as the critical shear stress of the ice-substrate interface is not the average shear stress (typically calculated as force divided by contact area), but the minimum shear stress.

It is usually not possible to measure the minimum shear stress directly, however, it can be calculated by knowing the Shear Stress Intensity Factor (SSIF) of the test bench (Table 3). This factor needs to be computed numerically for the test bench configuration and is defined as the average shear stress divided by the minimum shear stress. A similar stress concentration factor was introduced by Lou et al. [51]. Once the SSIF is known, it can be used to characterize any kind of solid surface, as it does not depend on the load applied. The SSIF only depends on the geometrical parameters of the test bench (ice diameter D, ice height H, and pushing height h). It will be sufficient to measure the average shear stress experimentally and know the SSIF to characterize the minimum shear stress of the ice-surface interface.

Table 3
Analysis of the shear stress values for four test cases with a mold of diameter $D = 8$ mm and ice height $H = 10$ mm. The Shear Stress Intensity Factor (SSIF) is defined as the average shear stress divided by the minimum shear stress and is found to not depend on the applied force, but only on the geometrical parameters of the test system (D, H, and h). Once the SSIFs for a certain test system are defined, it is possible to retrieve the values of the minimum shear stresses by measuring the average (F/A) shear stress values.

h [mm]	τ_{max} [kPa]	τ_{min} [kPa]	τ_{ave} [kPa]	SSIF [τ_{ave}/τ_{min}]
1	5460	588	1120	1,91
2	3317	646	1013	1,57
3	1874	675	883	1,31
4	1086	606	694	1,14
$\Delta\tau/\tau$	401%	14%	61%	

Experimentally, the stress-dominated fracture mechanism can be characterized by a sudden, instantaneous fracture and by a removal force that depends on the interface area. On the other hand, for a toughness-controlled fracture mechanism, the propagation of a crack along the interface is observed. In the latter case, the force required to debond the interface is independent of the ice sample size [52,53,55]. The experimental tests with sample size $D = 8$ mm have all shown a stress-dominated fracture behavior (refer to Fig. 6 and video in the SI). The question that now arises is what kind of stress is involved in the failure mechanism.

Fig. 4b shows the tensile stress results. Here, the curves follow a similar behavior in all 4 cases, with a relative difference of the maximum tensile stress of $\Delta\sigma_{max}/\sigma_{max} = 35\%$. σ shows a positive value (tension) only over half of the interface, while the remaining part is in a compression state. This is incompatible with a tensile stress-dominated fracture mechanism, given that, for the full detachment, the critical stress level needs to be reached over the entire interface. Keeping the above considerations in mind, the tensile stress cannot act as a failure criterion, as detachment always happens instantaneously over the full interface.

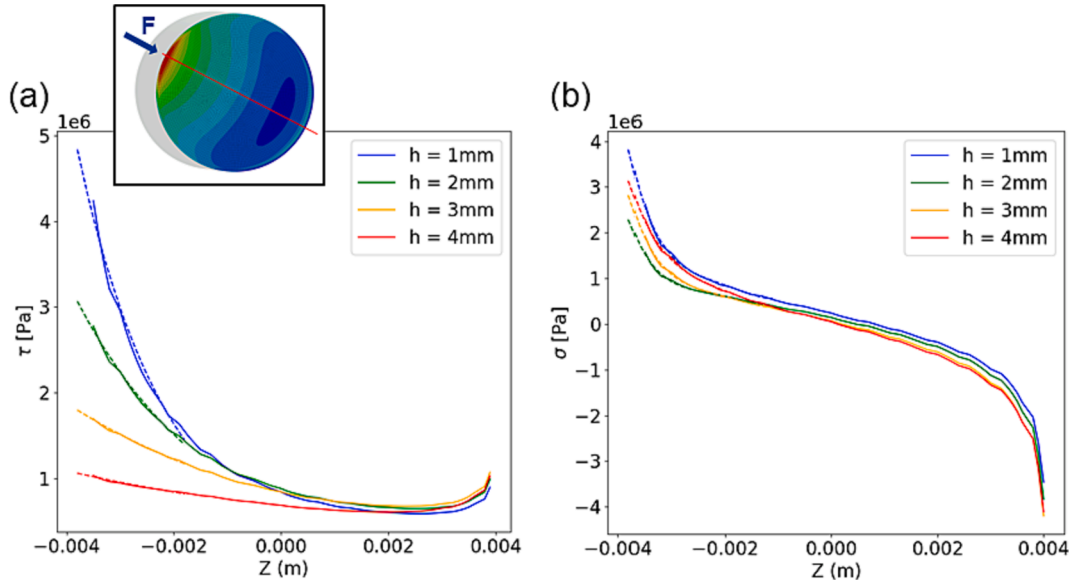

Fig. 4. Numerical calculations of the shear stress (a) and tensile stress (b) distribution along the symmetry line of the cylindrical ice samples with diameter $D = 8$ mm. Each line corresponds to the stress distribution at the experimentally determined maximum force. The dotted lines represent curve fittings for the stress values close to the force application point, as numerical mesh dependence was observed at Z = −0,004 m. Apart from the edge values, mesh independence was confirmed and presented in the SI (Section S5). Inset: shear stress distribution at the ice-substrate interface. The red line indicates the symmetry line from which the stress values were taken.

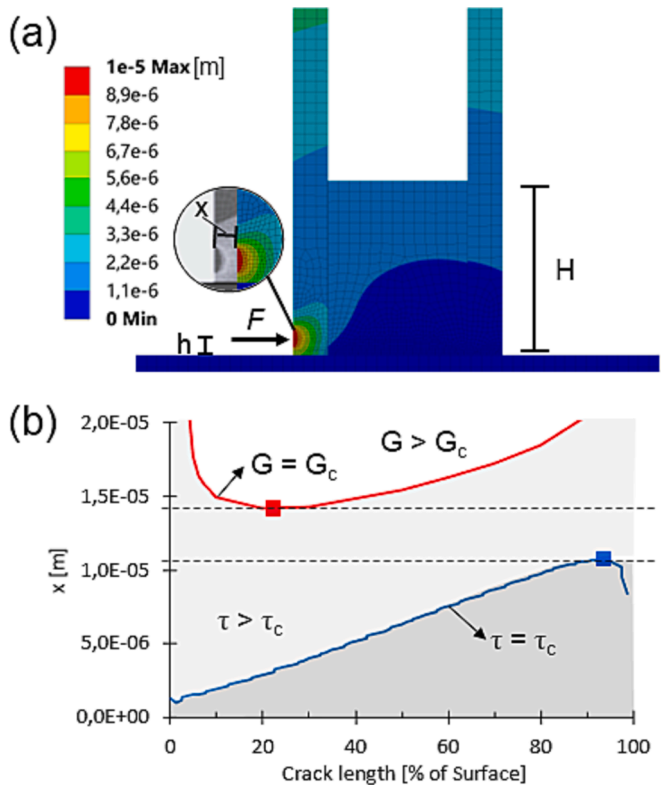

Fig. 5. (a) Numerical 2D analysis of the shear-stress and strain energy distribution. A force F is applied on the outside of the mold, similarly to the 3D model. The displacement while applying the force is denoted by x (see inset image). (b) Displacements x to reach the critical shear stress ($\tau_c = 600$ kPa) and the critical strain energy ($G_c = 3$ J/m^2) plotted for different crack lengths. For shear stress-dominated detachment, the point where the full surface reaches the critical shear stress (blue square) must be met before the critical strain energy is reached (red square). The theoretical derivation of this graph is presented in the SI (Section S6).

3.2. Fracture mechanism

The previous results are all obtained with a mold diameter $D = 8$ mm, for which all the experimental tests have shown a shear stress-dominated fracture behavior. The following analysis also considers the bigger mold size ($D = 14$ mm) and the critical strain energy to investigate the toughness-controlled fracture mechanism.

A 2D version of the previously presented numerical 3D model was used for this analysis (Fig. 5a). The mold thickness, the force application area, and the contact conditions were not changed. The numerical model provides the detailed shear stress and strain energy distribution, as a function of the applied force. For convenience, the following graphs are presented as a function of the displacement x imposed by the linear actuator. Displacement x and force F are, however, directly proportional (linear elastic model), and the result of the analysis does not change if reported as a function of F or x. By taking a critical shear stress of $\tau_c = 600kPa$ (determined in section 2.1) and a critical strain energy for an ice-aluminum interface of $G_c = 3J/m^2$ (for mode II detachment of freezer ice on aluminum substrate, value taken from [56]), it is then possible to draw the graph shown in Fig. 5b. Additional details on the theoretical derivation of this graph can be found in the SI (Section S6).

The plot compares the displacements x to reach the critical shear stress value (blue line) with the ones to reach the critical strain energy for different crack lengths (red line). If the displacement x required to reach the critical stress value over the entire surface of the ice sample (blue square in Fig. 5b) is smaller than the displacement required to reach the critical strain energy (red square in Fig. 5b), then the detachment is shear stress-dominated. Otherwise, there is a value of displacement for which the coupled criterion [52,65] is met and an initial partial crack corresponding to the minimum of the G_c curve will occur before the full detachment by stress [66]. The detachment will thus be toughness-dominated.

This 2D-version of the numerical model is used to investigate the four-fold difference of the average shear stress that is observed between the ice sample with $D = 8$ mm and $H = 5$ mm and the one with $D = 14$ mm and $H = 3$ mm (Fig. 3b, right plot). The simulation has been run for both geometries and the results are summarized in Fig. 6a and Fig. 6b.

In the case of the ice sample with diameter $D = 8$ mm, the simulations show that the stress condition for full detachment is indeed met before the critical strain energy condition (the blue square is reached for lower x than the red square). Therefore, the model predicts an instantaneous detachment of the entire ice-substrate interface. On the other hand, for the ice sample with $D = 14$ mm, slower crack propagation dominated by the critical strain energy is expected. This difference also explains the dissimilar average shear stress values obtained for the two cases, as in only one of the two cases the detachment is entirely controlled by the critical shear stress.

The presence of two different detachment mechanisms is verified

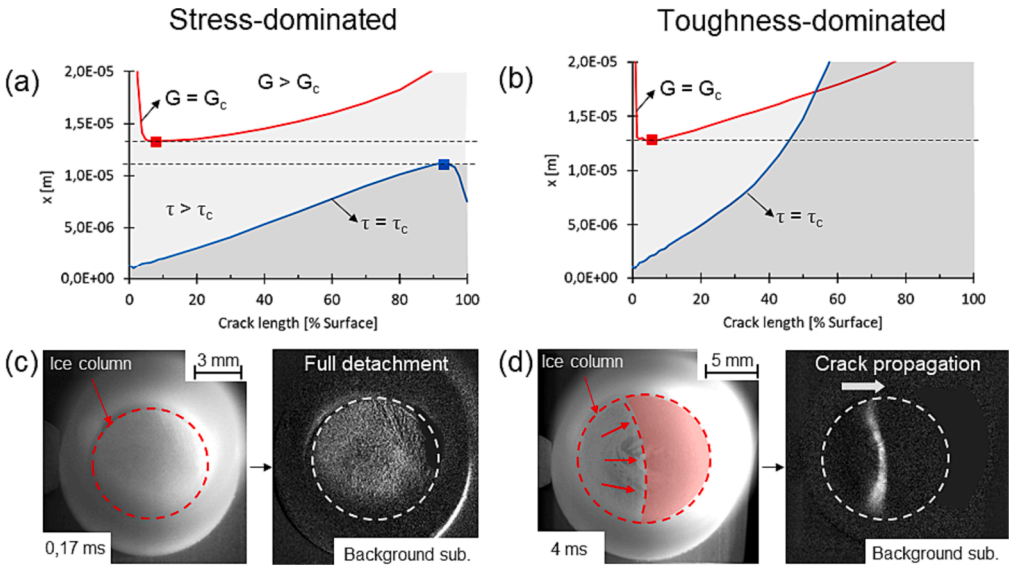

Fig. 6. Comparison of the displacements to reach the critical shear stress and critical strain energy for an ice sample with (a) $D = 8$ mm and $H = 5$ mm and with (b) $D = 14$ mm and $H = 3$ mm. (c) Experimentally visualized instantaneous crack of the entire ice-substrate interface (full detachment) for the ice sample with $D = 8$ mm and $H = 5$ mm. High-speed imaging and image subtraction allow visualizing a detachment of the entire surface in less than 0,17 ms. (d) Visualization of the crack propagation (partial detachment) for the $D = 14$ mm and $H = 3$ mm ice sample. The process from crack onset to complete detachment takes approximately 4 ms.

experimentally by using high-speed imagery (6000 fps) to visualize the crack propagation at the ice-substrate interface (Fig. 6c). Images are also presented with background subtraction (using the previous frame as background) to enhance the crack front visibility. In the case of the $D =$ 8 mm ice sample (Fig. 6c), the full detachment process takes less than 0,17 ms (1 frame) and the whole interface appears white in the subtracted image, which is typical for a stress-dominated detachment mechanism. On the contrary, for $D = 14$ mm (Fig. 6d), the crack propagation front is observed for the duration of 4 ms (24 frames) and only a minor part of the interface appears white on the subtracted image. This indicates a slower and gradual crack propagation, due to toughness-dominated detachment mechanism. The full videos can be found in the Supporting Information.

Note that the toughness-dominated detachment ($t \approx 4$ ms) is significantly slower than the stress-dominated detachment ($t < 0.17$ ms); however, both timescales are too low to be differentiated by eye in real-time. It is therefore essential, when performing the ice adhesion measurements with the push test, to be aware of the mechanism regime and report it together with the measured adhesion forces and stresses.

3.3. Optimization of the push test

The above results have been obtained by measuring ice adhesion on aluminum alloy, but most of the time this kind of push test is used to characterize the ice adhesion of novel coatings or surfaces, which have different critical strain energy (or toughness) and critical shear stress values. The above analysis has shown how even for relatively small ice samples ($D < 15$ mm), it is possible to be in a detachment regime governed by the critical strain energy and, therefore, the measured critical shear stresses can be misleading. To determine the critical shear stress of an interface with the method shown in section 2.1, it is necessary to stay in a regime of full instantaneous detachment. While testing different surface coatings with this test method, it could happen that the detachment mechanism changes and that the critical shear stress is no longer the minimum shear stress over the entire interface, but only over a fraction of it [52]. To this end, an optimization of the push test is carried out numerically, and practical suggestions are given to reduce the risk of partial detachment while determining the interface's critical shear stress.

The optimization analysis of the push test has been carried out for a mold with a diameter $D = 8$ mm, as it has previously been shown that with this mold size, it is possible to have a shear stress-dominated detachment. The goal of this analysis is to optimize the ice sample height H and the pushing height h, keeping all the other geometrical parameters constant. Fig. 7a shows the total strain energy in the ice sample for different crack lengths and different ice sample heights H, normalized by the square of the displacement x^2. It can be seen how more strain energy is accumulated in the ice for lower heights H. Due to this increased deformation, the critical strain is reached for lower displacements x, or, in other words, for lower pushing forces.

A lower ice height H also reflects on the shear stresses at the ice-substrate interface. As can be seen from Fig. 7b, bigger displacements x are required for $H = 2.5$ mm to reach the point where the full surface experiences the critical shear stress, compared to $H = 5$ mm or $H = 10$ mm. Thus, to facilitate stress-dominated detachment, the ice height H should be at least 5 mm for this case.

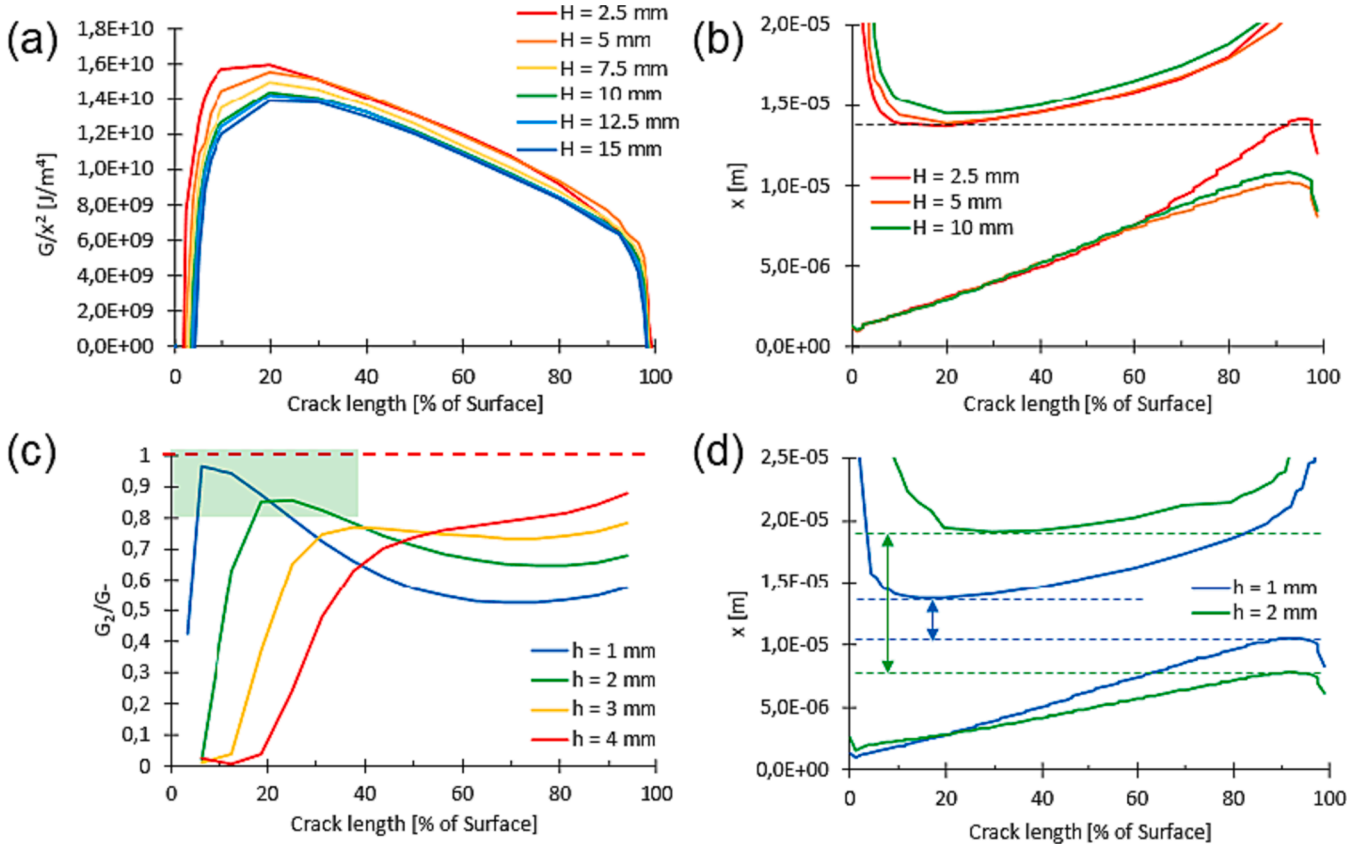

Fig. 7. (a) Strain energy in the ice sample normalized by the square of the displacement x^2 for different crack lengths and different ice sample heights H. The higher the strain energy, the more probable the detachment due to critical strain energy. (b) Displacements to reach the critical shear stress and the critical strain energy plotted versus the crack length for $D = 8$ mm, $h = 1$, and different ice sample heights H. (c) Mode II (sliding) failure energy (G_2) over the total (G_T) failure energy. The closer the value to 100% (red dotted line), the more dominant the second mode of failure. The relevant values are between 0 and 40% of crack length, where the minima of the critical strain energy are observed. (d) Displacements to reach the critical shear stress and the critical strain energy plotted versus the crack length for $D = 8$ mm, $H = 12.5$ mm, and different pushing heights h.

Before studying the influence of the pushing height h on critical shear stress and critical strain energy, it was important to verify up to which point the failure mode is dominated by a sliding motion (mode II) [64]. The reason for this is that the critical strain energy considered in this study ($G_c = 3J/m^2$) is valid only for mode II failure. The Virtual Crack Closure Technique (VCCT) allows investigating the contribution of each of the different crack opening modes, and therefore, comparing G_I to G_{II} strain energy. According to [56], the total strain energy G_T can be calculated as $G_T = G_I + G_{II}$, meaning that the closer G_{II}/G_T to 1, the higher the sliding component of the fracture.

Fig. 7c plots the value of G_{II}/G_T for different crack lengths and different pushing heights h. The area of the graph that is relevant to this study has been highlighted in light green. In this area, G_{II}/G_T is higher than 80% and, at the same time, the crack length is smaller than 40%. Considering only crack lengths below 40% is motivated by the fact that, in the previous analyses (Fig. 5b and Fig. 7b), the minimum critical strain energy is always found in this region. Only the cases $h = 1$ mm and $h = 2$ mm satisfy these conditions, while for the other two cases, the failure mode is generally a mixed opening mode and, therefore, not suitable for an analysis that assumes pure shear conditions.

By comparing the critical shear stress and critical strain energy for $h = 1$ mm and $h = 2$ mm (Fig. 7d), an interesting mechanism is revealed: by pushing the ice block at $h = 2$ mm, the critical strain energy at the interface is reached only at higher displacements x (Fig. 7d, the curve is pushed upwards). At higher pushing distances, the strain energy is accumulated more in the bulk of the ice cylinder and less at the ice-substrate interface. Simultaneously, the critical shear stress is reached for lower x, favoring a stress-dominated detachment.

In conclusion, to reduce the risk of partial detachment (as shown for example in Fig. 6d) and enable a more precise measurement of the interface's critical shear stress, the ice height H should be at least 5 mm, the diameter D should be kept ideally below 10 mm and the pushing height h should be comprised between 1 and 2 mm, preferably closer to 2 mm.

4. Conclusions

Assessing ice adhesion on solid surfaces is a crucial step in characterizing both standard materials and coatings designed to reduce ice adhesion. However, ice adhesion tests are often misunderstood: on one hand, the average shear stress, $\tau_{ave} = F/A$, measured during ice detachment, is confused with the critical shear stress, τ_c; on the other hand, tests are usually performed without clarifying the fracture mechanism (stress- or toughness-dominated).

In this study, we conducted complementary experimental and numerical investigations, for a traditional horizontal push test, the most commonly used ice adhesion measurement system, using aluminum as a reference substrate. By altering the test conditions, we demonstrated by high-speed camera visualization that ice detachment can occur through either stress-dominated or toughness-dominated mechanisms. In a stress-dominated mechanism, detachment occurs not when the average shear stress, F/A, exceeds a critical value, i.e., $\tau_{ave} > \tau_c$, as hypothesized in several studies, but when the critical stress is exceeded over the entire interface, $\tau_{min} > \tau_c$. Under a stress-dominated mechanism of ice detachment, the critical shear stress, τ_c, can be calculated by knowing the shear stress intensity factors (which are a characteristic of the measurement setup and the ice shape). These factors express the ratio between the average stress value, τ_{ave}, and the minimum stress value τ_{min}.

In contrast, in the case of a toughness-dominated mechanism, detachment is controlled by strain energy release instead of stress. Therefore, the determination of the critical shear stress, τ_c, is only meaningful under a stress-dominated detachment mechanism. Since the two mechanisms cannot be distinguished by eyes, experiments should be conducted with care, as the detachment time scales are too low, in the order of 0.1 ms and 1 ms for stress-dominated and toughness-dominated mechanisms, respectively.

As a practical guideline for the design of experiments, we have proposed a simple fracture model that facilitates differentiation between the two detachment regimes. Generally, the stress-dominated detachment regime can be favored by reducing the ice-block diameter, increasing the ice-block height, and spacing the distance between the force probe and substrate appropriately, as this reduces the strain energy accumulated at the ice-substrate interface.

To conclude, we aim to increase awareness of the common misunderstandings related to ice adhesion testing, with the objective of improving the reliability and reproducibility of tests. This is particularly relevant in the development and production of icephobic coatings and materials designed to reduce ice adhesion and contrast icing on solid surfaces.

Associated Content

Supporting information: Description of the experimental test system used for this study, additional details, validation, a mesh independence study for the numerical model, and additional analytical derivations (DOC). Two supplementary videos for the differentiation between fracture mechanisms are provided (mp4).

CRediT authorship contribution statement

Luca Stendardo: Conceptualization, Methodology, Validation, Formal analysis, Investigation, Writing – original draft, Visualization. **Giulia Gastaldo:** Methodology, Writing – original draft. **Marc Budinger:** Conceptualization, Methodology, Formal analysis, Writing – original draft, Supervision. **Valérie Pommier-Budinger:** Conceptualization, Methodology, Formal analysis, Writing – original draft, Supervision, Funding acquisition. **Irene Tagliaro:** Conceptualization, Writing – original draft, Supervision, Project administration. **Pablo F. Ibáñez-Ibáñez:** Conceptualization, Writing – original draft, Supervision. **Carlo Antonini:** Conceptualization, Methodology, Formal analysis, Writing – original draft, Supervision, Project administration, Funding acquisition.

Declaration of Competing Interest

The authors declare that they have no known competing financial interests or personal relationships that could have appeared to influence the work reported in this paper.

Data availability

Data will be made available on request.

Acknowledgments

This project has received funding from the European Union's Horizon 2020 research and innovation programme under the Marie Skłodowska-Curie grant agreement No 956703 (SURFICE Smart surface design for efficient ice protection and control). P.F.I.I. acknowledges the funding from the Margarita Salas grant (Ministerio de Universidades, Next Generation EU).

Appendix A. Supplementary data

Supplementary data to this article can be found online at https://doi.org/10.1016/j.apsusc.2023.158462.

References

[1] R.W. Gent, N.P. Dart, J.T. Cansdale, Aircraft icing, Philos. Trans. R. Soc. Lond. Ser. Math. Phys. Eng. Sci. 358 (1776) (Nov. 2000) 2873–2911, https://doi.org/10.1098/rsta.2000.0689.

[2] F.T. Lynch, A. Khodadoust, Effects of ice accretions on aircraft aerodynamics, Prog. Aerosp. Sci. 37 (8) (Nov. 2001) 669–767, https://doi.org/10.1016/S0376-0421(01)00018-5.

[3] W.C. Geer, M. Scott, The prevention of the ice hazard on airplanes, 1930.
[4] J.L. Laforte, M.A. Allaire, J. Laflamme, State-of-the-art on power line de-icing, Atmospheric Res. 46 (1–2) (Apr. 1998) 143–158, https://doi.org/10.1016/S0169-8095(97)00057-4.
[5] A.J. Meuler, J.D. Smith, K.K. Varanasi, J.M. Mabry, G.H. McKinley, R.E. Cohen, Relationships between water wettability and ice adhesion, ACS Appl. Mater. Interfaces 2 (11) (Nov. 2010) 3100–3110, https://doi.org/10.1021/am1006035.
[6] Z. Goraj, An Overview of the Deicing and Antiicing Technologies with Prospects for the Future. Presented at the 24th International Congress of the Aeronautical Sciences, 2004.
[7] Y. Shen, X. Wu, J. Tao, C. Zhu, Y. Lai, Z. Chen, Icephobic materials: Fundamentals, performance evaluation, and applications, Prog. Mater. Sci. 103 (Jun. 2019) 509–557, https://doi.org/10.1016/j.pmatsci.2019.03.004.
[8] I. Tagliaro, A. Cerpelloni, V.-M. Nikiforidis, R. Pillai, C. Antonini, On the Development of Icephobic Surfaces: Bridging Experiments and Simulations, in: M. Marengo, J. De Coninck (Eds.), The Surface Wettability Effect on Phase Change, Springer International Publishing, Cham, 2022, pp. 235–272, https://doi.org/10.1007/978-3-030-82992-6_8.
[9] M. Grizen, M.K. Tiwari, Icephobic Surfaces: Features and Challenges, in: K.L. Mittal, C. -H. Choi, (Eds.), Ice Adhesion, first ed., Wiley, 2020, pp. 417–466. doi: 10.1002/9781119640523.ch14.
[10] P. Irajizad, S. Nazifi, H. Ghasemi, Icephobic surfaces: Definition and figures of merit, Adv. Colloid Interface Sci. 269 (Jul. 2019) 203–218, https://doi.org/10.1016/j.cis.2019.04.005.
[11] Y. Zhuo, S. Xiao, A. Amirfazli, J. He, Z. Zhang, Polysiloxane as icephobic materials – The past, present and the future, Chem. Eng. J. 405 (Feb. 2021), 127088, https://doi.org/10.1016/j.cej.2020.127088.
[12] L. Bao, Z. Huang, N.V. Priezjev, S. Chen, K. Luo, H. Hu, A significant reduction of ice adhesion on nanostructured surfaces that consist of an array of single-walled carbon nanotubes: A molecular dynamics simulation study, Appl. Surf. Sci. 437 (Apr. 2018) 202–208, https://doi.org/10.1016/j.apsusc.2017.12.096.
[13] Q. Sun, Y. Zhao, K.-S. Choi, X. Hou, X. Mao, Reduction of atomistic ice tensile stress by graphene–carbon nanotube coating, Appl. Surf. Sci. 565 (Nov. 2021), 150562, https://doi.org/10.1016/j.apsusc.2021.150562.
[14] A. Amirfazli, C. Antonini, Fundamentals of Anti-Icing Surfaces, in: Non-wettable Surfaces: Theory, Preparation, and Applications, in RSC Soft Matter, no. 5. The Royal Society of Chemistry, 2017.
[15] R. Attarzadeh, A. Dolatabadi, Icephobic performance of superhydrophobic coatings: A numerical analysis, Int. J. Heat Mass Transf. 136 (Jun. 2019) 1327–1337, https://doi.org/10.1016/j.ijheatmasstransfer.2019.03.079.
[16] S. Miao, X. Liu, Y. Chen, Freezing as a path to build micro-nanostructured icephobic coatings, Adv. Funct. Mater. 33 (9) (Feb. 2023) 2212245, https://doi.org/10.1002/adfm.202212245.
[17] I.V. Roisman, C. Tropea, Wetting and icing of surfaces, Curr. Opin. Colloid Interface Sci. 53 (Jun. 2021), 101400, https://doi.org/10.1016/j.cocis.2020.101400.
[18] V. Vercillo, et al., Design rules for laser-treated icephobic metallic surfaces for aeronautic applications, Adv. Funct. Mater. 30 (16) (Apr. 2020) 1910268, https://doi.org/10.1002/adfm.201910268.
[19] L. Wang, et al., Superhydrophobic microstructures for better anti-icing performances: open-cell or closed-cell? Mater. Horiz. 10 (1) (2023) 209–220, https://doi.org/10.1039/D2MH01083F.
[20] C. Chen, et al., Micro–nano-nanowire triple structure-held PDMS superhydrophobic surfaces for robust ultra-long-term icephobic performance, ACS Appl. Mater. Interfaces 14 (20) (May 2022) 23973–23982, https://doi.org/10.1021/acsami.2c02992.
[21] C.H. Moon, et al., Icephobic coating through a self-formed superhydrophobic surface using a polymer and microsized particles, ACS Appl. Mater. Interfaces 14 (2) (Jan. 2022) 3334–3343, https://doi.org/10.1021/acsami.1c22404.
[22] Y. Li, et al., One-pot synthesis of superhydrophobic photothermal materials with self-healing for efficient ice removal, Appl. Surf. Sci. 600 (Oct. 2022), 154177, https://doi.org/10.1016/j.apsusc.2022.154177.
[23] V.Y. Lolla, S.F. Ahmadi, H. Park, A.P. Fugaro, J.B. Boreyko, Arrested dynamics of droplet spreading on ice, Phys. Rev. Lett. 129 (7) (Aug. 2022), 074502, https://doi.org/10.1103/PhysRevLett.129.074502.
[24] Y. Liu, Y. Wu, Y. Liu, R. Xu, S. Liu, F. Zhou, Robust Photothermal Coating Strategy for Efficient Ice Removal, ACS Appl. Mater. Interfaces 12 (41) (Oct. 2020) 46981–46990, https://doi.org/10.1021/acsami.0c13367.
[25] T. Li, et al., Self-Deicing Electrolyte Hydrogel Surfaces with Pa-level Ice Adhesion and Durable Antifreezing/Antifrost Performance, ACS Appl. Mater. Interfaces 12 (31) (Aug. 2020) 35572–35578, https://doi.org/10.1021/acsami.0c06912.
[26] Y. Liu, T. Wang, Z. Song, M. Chen, Spreading and freezing of supercooled water droplets impacting an ice surface, Appl. Surf. Sci. 583 (May 2022), 152374, https://doi.org/10.1016/j.apsusc.2021.152374.
[27] S. Qin, Y. Jin, F. Yin, Z. Wang, G. Bai, Can solid surface energy be a predictor of ice nucleation ability? Appl. Surf. Sci. 602 (Nov. 2022), 154193 https://doi.org/10.1016/j.apsusc.2022.154193.
[28] P. F. Ibáñez-Ibáñez, F. J. Montes Ruiz-Cabello, M. A. Cabrerizo-Vílchez, and M. A. Rodríguez-Valverde, "Ice adhesion of PDMS surfaces with balanced elastic and water-repellent properties," *J. Colloid Interface Sci.*, vol. 608, pp. 792–799, Feb. 2022, doi: 10.1016/j.jcis.2021.10.005.
[29] V. Donadei, H. Koivuluoto, E. Sarlin, P. Vuoristo, Icephobic Behaviour and Thermal Stability of Flame-Sprayed Polyethylene Coating: The Effect of Process Parameters, J. Therm. Spray Technol. 29 (1–2) (Jan. 2020) 241–254, https://doi.org/10.1007/s11666-019-00947-0.
[30] Y. Ibrahim, R. Kempers, A. Amirfazli, 3D printed electro-thermal anti- or de-icing system for composite panels, Cold Reg. Sci. Technol. 166 (Oct. 2019), 102844, https://doi.org/10.1016/j.coldregions.2019.102844.
[31] J. Liu, et al., Hydrophobic/icephobic coatings based on thermal sprayed metallic layers with subsequent surface functionalization, Surf. Coat. Technol. 357 (Jan. 2019) 267–272, https://doi.org/10.1016/j.surfcoat.2018.10.002.
[32] V. Palanque, "Design of low consumption electro-mechanical de-icing systems", Engineering Sciences [physics], Université de Toulouse, ISAE-Supaero, 2022.
[33] L. Snels, et al., Internal and interfacial microstructure characterization of ice droplets on surfaces by X-ray computed tomography, J. Colloid Interface Sci. 637 (May 2023) 500–512, https://doi.org/10.1016/j.jcis.2023.01.103.
[34] C. Wu, et al., Highly efficient solar anti-icing/deicing *via* a hierarchical structured surface, Mater. Horiz. 7 (8) (2020) 2097–2104, https://doi.org/10.1039/D0MH00636J.
[35] K. Regulagadda, J. Gerber, T.M. Schutzius, D. Poulikakos, Microscale investigation on interfacial slippage and detachment of ice from soft materials, Mater. Horiz. 9 (4) (2022) 1222–1231, https://doi.org/10.1039/D1MH01993G.
[36] F. Wang, S. Xiao, Y. Zhuo, W. Ding, J. He, Z. Zhang, Liquid layer generators for excellent icephobicity at extremely low temperatures, Mater. Horiz. 6 (10) (2019) 2063–2072, https://doi.org/10.1039/C9MH00859D.
[37] J.H. Kim, M.J. Kim, B. Lee, J.M. Chun, V. Patil, Y.-S. Kim, Durable ice-lubricating surfaces based on polydimethylsiloxane embedded silicone oil infused silica aerogel, Appl. Surf. Sci. 512 (May 2020), 145728, https://doi.org/10.1016/j.apsusc.2020.145728.
[38] Z. He, Y. Zhuo, Z. Zhang, J. He, Design of Icephobic Surfaces by Lowering Ice Adhesion Strength: A Mini Review, Coatings 11 (11) (Nov. 2021) 1343, https://doi.org/10.3390/coatings11111343.
[39] C. Chen, et al., Crack-Initiated Durable Low-Adhesion Trilayer Icephobic Surfaces with Microcone-Array Anchored Porous Sponges and Polydimethylsiloxane Cover, ACS Appl. Mater. Interfaces 15 (4) (Feb. 2023) 6025–6034, https://doi.org/10.1021/acsami.2c15483.
[40] S. Nazifi, Z. Huang, A. Hakimian, H. Ghasemi, Fracture-controlled surfaces as extremely durable ice-shedding materials, Mater. Horiz. 9 (10) (2022) 2524–2532, https://doi.org/10.1039/D2MH00619G.
[41] Y. Zhuo, et al., Gels as emerging anti-icing materials: a mini review, Mater. Horiz. 8 (12) (2021) 3266–3280, https://doi.org/10.1039/D1MH00910A.
[42] P. Irajizad, et al., Stress-localized durable icephobic surfaces, Mater. Horiz. 6 (4) (2019) 758–766, https://doi.org/10.1039/C8MH01291A.
[43] H. Zheng, G. Liu, B.B. Nienhaus, J.V. Buddingh, Ice-Shedding Polymer Coatings with High Hardness but Low Ice Adhesion, ACS Appl. Mater. Interfaces 14 (4) (Feb. 2022) 6071–6082, https://doi.org/10.1021/acsami.1c23483.
[44] A. Work, Y. Lian, A critical review of the measurement of ice adhesion to solid substrates, Prog. Aerosp. Sci. 98 (Apr. 2018) 1–26, https://doi.org/10.1016/j.paerosci.2018.03.001.
[45] S. Rønneberg, J. He, Z. Zhang, The need for standards in low ice adhesion surface research: a critical review, J. Adhes. Sci. Technol. 34 (3) (Feb. 2020) 319–347, https://doi.org/10.1080/01694243.2019.1679523.
[46] Y. Wang, et al., Organogel as durable anti-icing coatings, Sci. China Mater. 58 (7) (Jul. 2015) 559–565, https://doi.org/10.1007/s40843-015-0069-7.
[47] T. Maitra, S. Jung, M.E. Giger, V. Kandrical, T. Ruesch, D. Poulikakos, Superhydrophobicity vs. Ice Adhesion: The Quandary of Robust Icephobic Surface Design, Adv. Mater. Interfaces 2 (16) (Nov. 2015) 1500330, https://doi.org/10.1002/admi.201500330.
[48] F. Tarpoudi Baheri, L.D. Poulikakos, D. Poulikakos, T.M. Schutzius, Ice adhesion behavior of heterogeneous bituminous surfaces, Cold Reg. Sci. Technol. 192 (Dec. 2021), 103405, https://doi.org/10.1016/j.coldregions.2021.103405.
[49] C. Wang, W. Zhang, A. Siva, D. Tiea, K.J. Wynne, Laboratory Test for Ice Adhesion Strength Using Commercial Instrumentation, Langmuir 30 (2) (Jan. 2014) 540–547, https://doi.org/10.1021/la4044254.
[50] L. Makkonen, Ice Adhesion —Theory, Measurements and Countermeasures, J. Adhes. Sci. Technol. 26 (4–5) (Mar. 2012) 413–445, https://doi.org/10.1163/016942411X574583.
[51] D. Lou, D. Hammond, M.-L. Pervier, Investigation of the Adhesive Properties of the Ice-Aluminum Interface, J. Aircr. 51 (3) (May 2014) 1051–1056, https://doi.org/10.2514/1.C032509.
[52] E. Martin, T. Vandellos, D. Leguillon, N. Carrère, Initiation of edge debonding: coupled criterion versus cohesive zone model, Int. J. Fract. 199 (2) (Jun. 2016) 157–168, https://doi.org/10.1007/s10704-016-0101-2.
[53] K. Golovin, A. Dhyani, M.D. Thouless, A. Tuteja, Low–interfacial toughness materials for effective large-scale deicing, Science 364 (6438) (Apr. 2019) 371–375, https://doi.org/10.1126/science.aav1266.
[54] Giulia Gastaldo, Valerian Palanque, Marc Budinger, and Valerie Pommier-Budinger, "Stress and Energy Release Rate Influence on Ice Shedding with Resonant Electro-Mechanical De-Icing Systems," presented at the ICAS 2022 - 33rd Congress of the International Council of the Aeronautical Sciences, Stockholm, Sweden, Sep. 2022. [Online]. Available: hal-03823920.
[55] D. Leguillon, Strength or toughness? A criterion for crack onset at a notch, Eur. J. Mech. - ASolids 21 (1) (Jan. 2002) 61–72, https://doi.org/10.1016/S0997-7538(01)01184-6.
[56] M. Huré, P. Olivier, J. Garcia, Effect of Cassie-Baxter versus Wenzel states on ice adhesion: A fracture toughness approach, Cold Reg. Sci. Technol. 194 (Feb. 2022), 103440, https://doi.org/10.1016/j.coldregions.2021.103440.
[57] Z. Azimi Dijvejin, M.C. Jain, R. Kozak, M.H. Zarifi, K. Golovin, Smart low interfacial toughness coatings for on-demand de-icing without melting, Nat. Commun. 13 (1) (Aug. 2022) 5119, https://doi.org/10.1038/s41467-022-32852-6.

[58] M. Mohseni, L. Recla, J. Mora, P.G. Gallego, A. Agüero, K. Golovin, Quasicrystalline Coatings Exhibit Durable Low Interfacial Toughness with Ice, ACS Appl. Mater. Interfaces 13 (30) (Aug. 2021) 36517–36526, https://doi.org/10.1021/acsami.1c08740.
[59] W.C. Macklin, The density and structure of ice formed by accretion, Q. J. R. Meteorol. Soc. 88 (375) (Jan. 1962) 30–50, https://doi.org/10.1002/qj.49708837504.
[60] V. Palanque, E. Villeneuve, M. Budinger, V. Pommier-Budinger, G. Momen, Cohesive strength and fracture toughness of atmospheric ice, Cold Reg. Sci. Technol. 204 (Dec. 2022), 103679, https://doi.org/10.1016/j.coldregions.2022.103679.
[61] N. Perez, "Linear-Elastic Fracture Mechanics", in *Fracture Mechanics*, Springer International Publishing, Cham, 2017, pp. 79–130.
[62] R. Krueger, Virtual crack closure technique: History, approach, and applications, Appl. Mech. Rev. 57 (2) (Mar. 2004) 109–143, https://doi.org/10.1115/1.1595677.
[63] Q. Yang, B. Cox, Cohesive models for damage evolution in laminated composites, Int. J. Fract. 133 (2) (May 2005) 107–137, https://doi.org/10.1007/s10704-005-4729-6.
[64] J.R. Reeder, An Evaluation of Mixed-Mode Delamination Failure Criteria, NASA, Feb. 1992.
[65] E. Martin, D. Leguillon, A strain energy density criterion for the initiation of edge debonding, Theor. Appl. Fract. Mech. 79 (Oct. 2015) 58–61, https://doi.org/10.1016/j.tafmec.2015.06.011.
[66] Z. Hashin, Finite thermoelastic fracture criterion with application to laminate cracking analysis, J. Mech. Phys. Solids 44 (7) (Jul. 1996) 1129–1145, https://doi.org/10.1016/0022-5096(95)00080-1.